Desalination and Water Treatment
www.deswater.com

doi: 10.5004/dwt.2019.24774

171 (2019) 344–355
December

Silver-mediated Bi_2O_3 and graphitic carbon nitride nanocomposite as all solid state Z scheme photocatalyst for imidacloprid pesticide abatement from water

Pankaj Raizada[a,b,*], Anita Sudhaik[a], Pardeep Singh[a], Ahmad Hosseini-Bandegharaei[b,c], Vinod Kumar Gupta[d], Shilpi Agarwal[d]

[a]*School of Chemistry, Faculty of Basic Sciences, Shoolini University, Solan(HP)-173229, India, Tel. +91-1792-308000; Fax: +91-1792-308000; emails: pankajchem1@gmail.com (P. Raizada), sudhaikanita@gmail.com (A. Sudhaik), pardeepchem@gmail.com (P. Singh)*
[b]*Department of Environmental Health Engineering, Faculty of Health, Sabzevar University of Medical Sciences, Sabzevar, Iran, email: ahoseinib@yahoo.com*
[c]*Department of Engineering, Kashmar Branch, Islamic Azad University, P.O. Box: 161, Kashmar, Iran*
[d]*Department of Biological Sciences, Faculty of Science, King Abdulaziz University, Jeddah, Saudi Arabia, emails: vinodfcy@gmail.com (V.K. Gupta), shilpi.agarwal2307@gmail.com (S. Agarwal)*

Received 27 March 2019; Accepted 7 August 2019

ABSTRACT

Herein, Ag-anchored Bi_2O_3/g-C_3N_4 based Z-scheme photocatalyst was prepared using facile hydrothermal approach for photocatalytic degradation of imidacloprid pesticide (IMP). Graphitic carbon nitride (GCN) nanocomposites were fabricated via thermal polycondensation and Ag-anchored Bi_2O_3/g-C_3N_4 (Ag-BO/GCN) via single-step hydrothermal method, respectively. The spectral analysis such as XRD, SEM, TEM, IR, PL, UV and XPS and BET were performed to investigate physicochemical properties of Ag-BO/GCN. The enhanced catalytic performance of Ag-BO/GCN was benefited from complimentary transport and separation efficacy of photogenerated electron–hole pairs via Z scheme pathway. The synthesized Ag-BO/GCN exhibited remarkable imidacloprid degradation (93%) than Ag-BO and GCN. The complete mineralization was attainted in 10 h under visible light irradiation. The improved photocatalytic activity of Ag-BO/GCN composites was credited to suitable band alignment between GCN and BO as well as presence of Ag (0) that acted as electron mediator thereby suppressing recombination between photoinduced charge carriers. The photocatalytic degradation of IMP followed pseudo-first order kinetics. The significant recyclability and stability of Ag-BO/GCN was observed for 10 catalytic cycles.

Keywords: Ag-anchored Bi_2O_3; Grpahitic carbon nitride; Heterojuction formation; Photocatalysis; Imidacloprid pesticide degradation

1. Introduction

Currently, environmental pollution and energy crises have become two major challenges [1]. Especially water pollution has emerged as a serious threat to environment because of accumulation of dyes, aromatics, hormones and pesticides in water resources. Worldwide these pollutants have attracted foremost attention because they are highly unbiodegradable toxic species and potentially able to be transformed into carcinogenic, teratogenic and even mutagenic agent. For this, bimetallic heterojunction was designed in the form of an interface integrating different semiconductor materials with suitable band edges promoting interfacial charge transfer and improving photoinduced charge carrier separation [2]. In 1972, TiO_2 was utilized for water

* Corresponding author.

splitting and exhibited unique properties such as high photocatalytic efficiency and good stability [3]. Lately, variety of semiconductor heterojunction in the form of photocatalysts, such as TiO_2/CdS [4] and g-C_3N_4–TaON [5], were designed. The photocatalysis emerged as a potential water remediation technique involving eradication of biotic/abiotic pollutants from aqueous phase. Upon light illumination, excited photocatalyst generates photogenerated charge carriers (e)/(h) [6]. Subsequently, few separated electron–hole pairs were transformed into hydroxyl radicals ($^{\bullet}OH$) and superoxide radicals ($^{\bullet}O_2^-$). The holes (h^+), $^{\bullet}OH$ and $^{\bullet}O_2^{-\bullet}$ as strong oxidizing species play vital part in water treatment. But, photocatalytic performance of photocatalyst depends upon some essential factors, that is, restricted visible light absorption and quick electron–hole pair recombination [7,8]. Congruously, construction of a highly efficient photocatalytic system possessing broad spectral response with potential electron–hole pair separation is vital. Designed photocatalyst should be stable, economical, abundant and less toxic [9]. In this regard, Bi_2O_3 (BO) candidatures a direct band gap semiconductor with band gap of 2.8 eV, utilizes visible light spectrum [10]. With a band gap of 2.8 eV, BO shows absorption band at 440 nm [11] and represents oxidation type semiconductor material. The conduction band (CB) and valence band (VB) of BO were corresponded to 0.33 and 3.13 V vs. NHE signifying high oxidation and weak reduction potential relative to positive CB and VB band edges [12]. BO displayed several dye degradation including Rhodamine B, orange G [13], methyl orange [14]. The various heterojunction systems comprising of BiOCl/BO [15], $BiVO_4$/BO [16] and BO/TiO_2 [17] were fabricated for the progression of photocatalytic performance.

Lately, graphitic carbon nitride (g-C_3N_4), a metal-free polymeric semiconductor material was discovered which is a stable allotrope of carbon nitride materials under normal reaction conditions. g-C_3N_4 appears as a photocatalytic agent for wastewater treatment in the presence of solar light [18,19]. g-C_3N_4, a solar light assisted semiconductor (2.7 eV band gap), has unique advantages including thermal and chemical stability [20,21]. Instead of its good properties, photocatalytic efficacy of g-C_3N_4 is hindered with some demerits, that is, high recombination rate of photogenerated electron–hole pairs, decreased surface area and restricted visible light response [22]. Lately, several strategies have been employed to expand quantum yield of g-C_3N_4 such as fabricating nanoporous structures, doping and heterojunction construction [23].

g-C_3N_4 (GCN) and BO photocatalyst exhibited upmost photocatalytic degradation activity employing Ag as an electron acceptor which minimizes photogenerated electron–hole pair recombination. In the present work, Ag-anchored BO/GCN nanohybrid with enhanced solar light response was synthesized and used for imidacloprid degradation. Heterojunction of Ag-anchored BO with GCN leads to photoinduced electron–hole pair separation and improves visible light absorption. In Z scheme mechanism, Ag plays a vital role in storing and conduction of electron and acted as a solid-state electron intermediary for channelling electrons from conduction band of BO to the valence band of GCN [24]. The effect of various reaction parameters such as IMP concentration, catalyst dose and pH was also explored with mechansicntic view of silver-mediated Z-scheme photocatalytic process.

2. Experimental

2.1. Materials and methods

Melamine ($C_3H_6N_6$), silver nitrate ($AgNO_3$) and bismuth nitrate pentahydrate [$Bi(NO_3)_3.5H_2O$] were procured from Sigma-Aldrich (India). Nitric acid (HNO_3), SDBS (sodium dodecyl benzene sulfonate) and sodium hydroxide (NaOH) were procured from Ranbaxy (India). Deionized water was employed for making all solutions used in experimental studies.

2.2. Preparation of GCN

Graphitic carbon nitride (GCN) was fabricated via thermal poly-condensation procedure using melamine, a nitrogen-rich precursor of GCN as starting material. Typically, 5 g of melamine was grounded in pestle and mortar and poured into a ceramic crucible covered with a lid. The crucible containing melamine was placed in muffle furnace and calcined at different temperature with ramping rate of 20°C/min up to 550°C for 4 h. After 4 h calcination, light yellowish powder was obtained, collected and cooled at room temperature. The resultant product was grounded into fine powder form and was labelled as GCN.

2.3. Synthesis of Ag-BO/GCN nanocomposite

In a typical synthesis of Ag-BO/GCN nanocomposite, 9.7 g $Bi(NO_3)_3.5H_2O$ and 0.034 g $AgNO_3$ were completely dissolved in 20 mL concentrated HNO_3 (2 mol L^{-1}) at 30°C. The whole reaction mixture was vigorously stirred magnetically to form a transparent aqueous solution of Bi^{3+} and Ag^+. During the synthesis process, amount of Ag^+ ions was incorporated into Bi_2O_3 lattice and obtained residue reacted with NaOH to produce AgOH. Thus metallic Ag was attained after a series of reactions and the reaction processes can be described as follows:

$$Ag^+ + OH^- \rightarrow AgOH \quad \text{(i)}$$

$$2AgOH \rightarrow Ag_2O + H_2O \quad \text{(ii)}$$

$$2Ag_2O \rightarrow 4Ag + O_2 \quad \text{(iii)}$$

In another beaker, the above-synthesized GCN powder (1 g) was dissolved in 30 mL deionized water followed by ultrasonication for 20 min. The resultant GCN solution was slowly added to the above-formed reaction solution with continuous magnetic stirring for half an hour. After that 0.05 g SDBS (sodium dodecyl benzene sulfonate) was dissolved in 20 mL deionized water and added dropwise to obtain reaction mixture under continuous stirring followed by addition of 4 mol L^{-1} NaOH solution to adjust pH to 11 with magnetic stirring for 3 h at 40°C. The resultant solution was then kept for 4 h at room temperature, centrifuged, washed several times with water and ethanol as well as dried

in oven at 80°C for 6 h. The obtained product was calcined at 500°C in muffle furnace for 2 h. After calcination, attained solid product was cooled, crushed into fine powder form and labelled as Ag-BO/GCN nanocomposites. Ag-anchored BO (Ag-BO) was synthesized via same procedure without the addition of GCN.

2.4. Photocatalytic experiment for IMP photodegradation

To evaluate Ag-BO/GCN nanocomposites photocatalytic activity, imidacloprid pesticide was selected as a target pollutant. The degradation process was carried in a slurry type photoreactor under LED light, as reported in previous work [25,26]. The slurry composed of imidacloprid and Ag-BO/GCN photocatalyst suspension was magnetically stirred throughout photocatalytic experiments. Aliquot (2 mL) was withdrawn, centrifuged and analyzed spectrophotometrically at 270 nm. The closed reflux method was also applied for chemical oxygen demand (COD) investigation [27]. Phenolphthalein was used as an indicator during titration of sample with NaOH to scrutinize dissolved carbon dioxide (CO_2). The photocatalytic efficiency was anticipated by means of the following equation [28]:

$$\%\ \text{removal effciency} = \frac{C_0 - C_t}{C_0} \times 100 \quad (1)$$

where C_0 is initial concentration of sample/COD and C_t is instant concentration of sample/COD in reaction solution. All the experiments were undertaken in triplicate with errors below 5% and average values were recorded.

3. Results and discussion

3.1. Characterization of Ag-BO/GCN nanocomposite

The morphology of GCN, Ag-anchored BO, Ag-BO/GCN photocatalysts was analyzed using FESEM technique. In Figs. 1a and b, graphitic carbon nitride exposed rough, irregular and porous sheet-like surface. In case of Ag-BO, accumulation of dopant (Ag) onto BO plates was clearly seen in FESEM images (Figs. 1c and d). Figs. 1e and f images clearly revealed dispersion of Ag-BO onto GCN sheets and indicated successful formation of Ag-BO/GCN nanocomposite. The dispersion state and structure of GCN, Ag-BO and Ag-BO/GCN was further investigated by TEM and HRTEM micrographs. Fig. 2a displays a sheet-like thin structure of

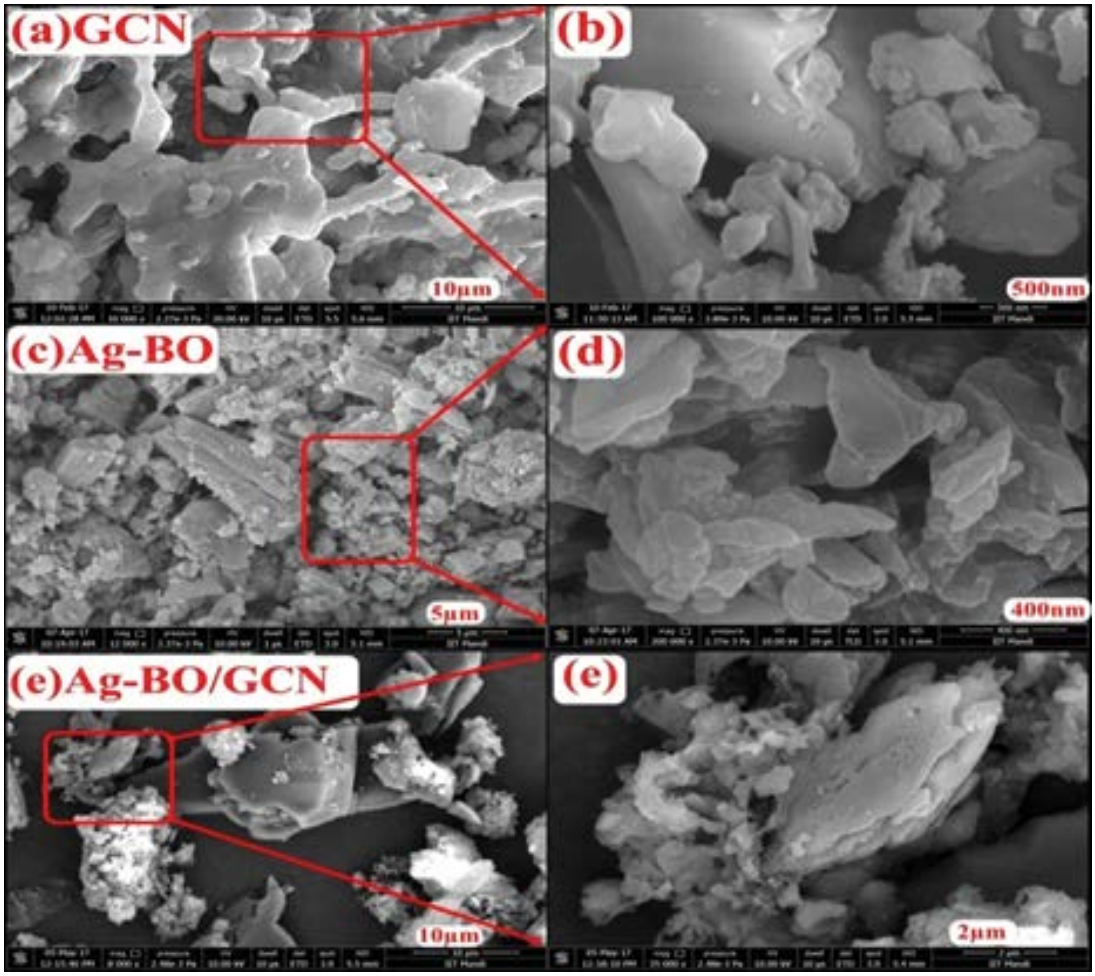

Fig. 1. FESEM images of GCN, BO and Ag-BO/GCN (a, c and e). (b), (d) and (f) are high resolution images of selected area with respective FESEM images.

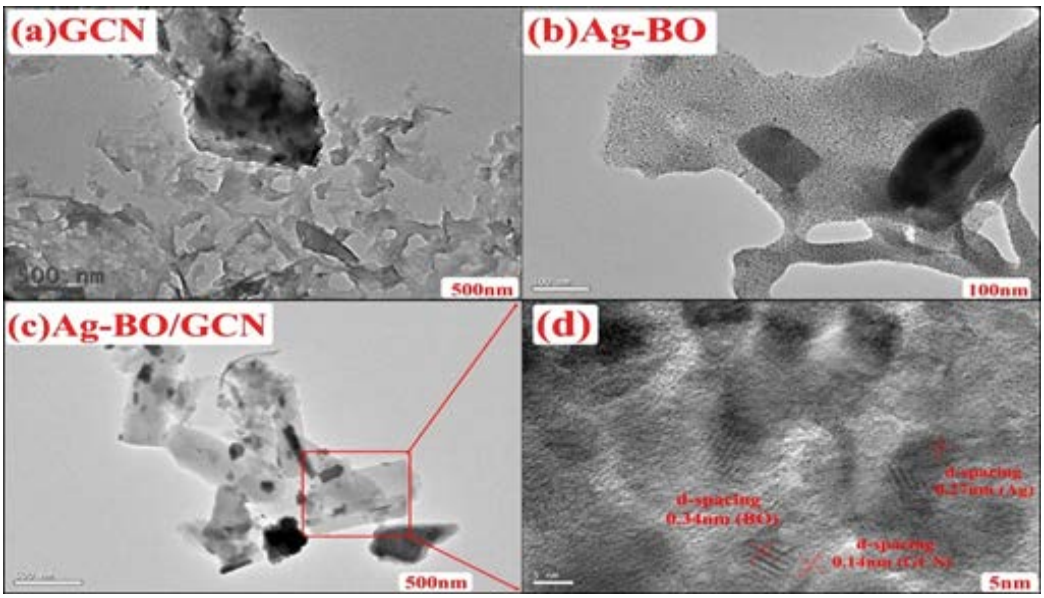

Fig. 2. TEM images of GCN (a), Ag-BO (b), Ag-BO/GCN (c) and (d) is HRTEM image of selected area of (c).

GCN which was composed of nanosheets [29]. In Fig. 2b, dark intense Ag particles were decorated on BO surface and were clearly seen in Ag-anchored BO nanosheets. In Ag-BO/GCN nanocomposite, Ag-anchored BO dark nanoparticles were dispersed on the surface of GCN shown in Fig. 2c [30]. HRTEM image of selected area of Fig. 2c is shown in Fig. 2d. It revealed lattice fringes with d-spacing of 0.14, 0.34 and 0.27 nm for GCN, BO and Ag, respectively [31].

Fig. S1 displayed EDAX spectra of GCN, BO, Ag-BO/GCN photocatalysts and confirmed the presence of C, N, Bi, O and Ag elements which confirmed the successful formation of synthesized photocatalysts. Fig. 3 shows XRD patterns of GCN, BO and Ag-BO/GCN nanocomposites. Two major peaks positioned at 13.04° and 27.74° corresponded to in-plane structural packing and inter-layer stacking of aromatic ring [32,33]. These two peaks were ascribed to (100) and (002) crystal planes of graphitic materials (JCPDS 87-1526) [34]. All diffraction peaks of BO were attributed to monoclinic phase and displayed crystalline nature of synthesized sample. The characteristic peaks at 2θ of 23.84°, 28.42°, 33.42° were associated to (120), (200) and (121) plane, respectively (JCPDS41-1449) [35]. In addition, a typical pattern of metallic Ag was also observed in Ag-BO/GCN nanocomposite that confirmed the formation of Ag-anchored BO. The peaks at 2θ of 27.65°, 31.93° and 45.95° were credited to (210), (113) and (124) crystal planes of Ag (JCPDS No. 00-004-0783) [36]. XRD patterns of Ag-BO/GCN nanocomposites exhibited diffraction peaks at 13.04°, 23.84°, 27.47°, 28.42°, 31.93°, 33.42° and 45.35° resembled to GCN, monoclinic BO and Ag.

The FTIR spectra of GCN, Ag-BO and Ag-BO/GCN were recorded between 400 and 4,000 cm^{-1} wavenumber (Fig. 4) [37]. The aromatic C-N stretching was recorded in region of 1,252–1,640 cm^{-1} [38]. The bending mode of heptazine rings was recorded at 810 cm^{-1}. A group of broad peaks were perceived in the range 3,200–3,400 cm^{-1} corresponded to stretching vibration of N–H bonds of primary amine

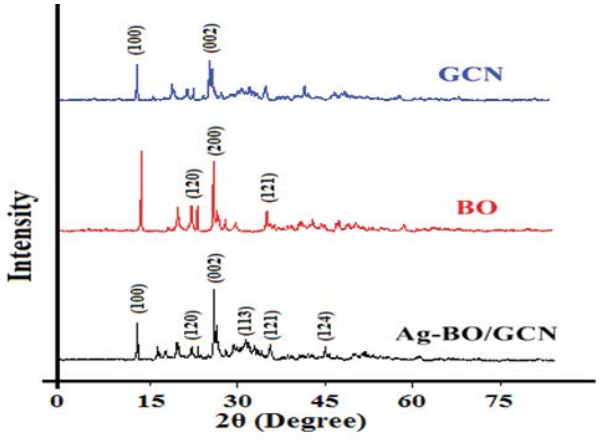

Fig. 3. XRD patterns of GCN, BO and Ag-BO/GCN photocatalyst.

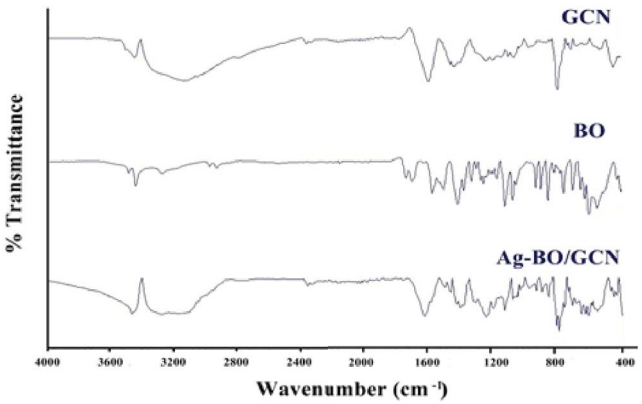

Fig. 4. FTIR spectra of GCN, BO and Ag-BO/GCN.

(–NH_2) [39]. In BO, absorption band in 200–800 cm^{-1} range was accredited to stretching vibration mode of Bi-O with mean wavenumber and intensity of bands. Bi-O formation was confirmed by absorption bands at 541, 503 and 430 cm^{-1} [40–42]. The peaks at 862, 762 and 903 cm^{-1} corresponded to stretching vibration of Bi-O-Bi [43]. The bands at 3,440 and 1,400 cm^{-1} indicated existence of O-H stretching of absorbed H_2O molecules [44]. The peaks at 900 to 1,383 cm^{-1} were assigned to Bi-O-Ag stretching vibrations in Ag-BO/GCN nanocomposite [36,43,44].

XPS analysis was used to elucidate the chemical state and surface chemical composition of prepared samples. Fig. 5 displays the survey scan XPS spectra of Ag-anchored BO/GCN nanocomposite and revealed the presence of C, N, Ag, Bi and O elements in the prepared composite deprived of other element signals presence. Fig. 5a presents XPS analysis of C 1s with peaks focused at 283 and 287.2 eV, respectively. The peak at 283 eV was allocated to carbon atoms (C–C bonding) and indicated the presence of amorphous carbon in Ag-BO/GCN nanocomposite surface [45]. However, peak at 287.2 eV was recognized as sp^2-bonded carbon (N–C–N). Fig. 5b exposed N 1s spectrum and a peak at 398 eV was observed that was associated to sp^2-bonded N atom in triazine rings (C–N–C). Fig. 5c exposes binding energy values of Ag ($3d_{5/2}$) and Ag ($3d_{3/2}$), that is, 368 and 374.3 eV, respectively and these binding energy values confirmed the existence of Ag in metallic state in synthesized Ag-BO/GCN nanocomposites [46]. XPS spectrum of Bi 4f is shown in Fig. 5d where two peaks with binding energies of 158.6 and 164.5 eV were evidently observed and were corresponded to Bi $4f_{7/2}$ and Bi $4f_{5/2}$, respectively, signifying the presence of Bi species in Bi^{3+} ion form in nanocomposite

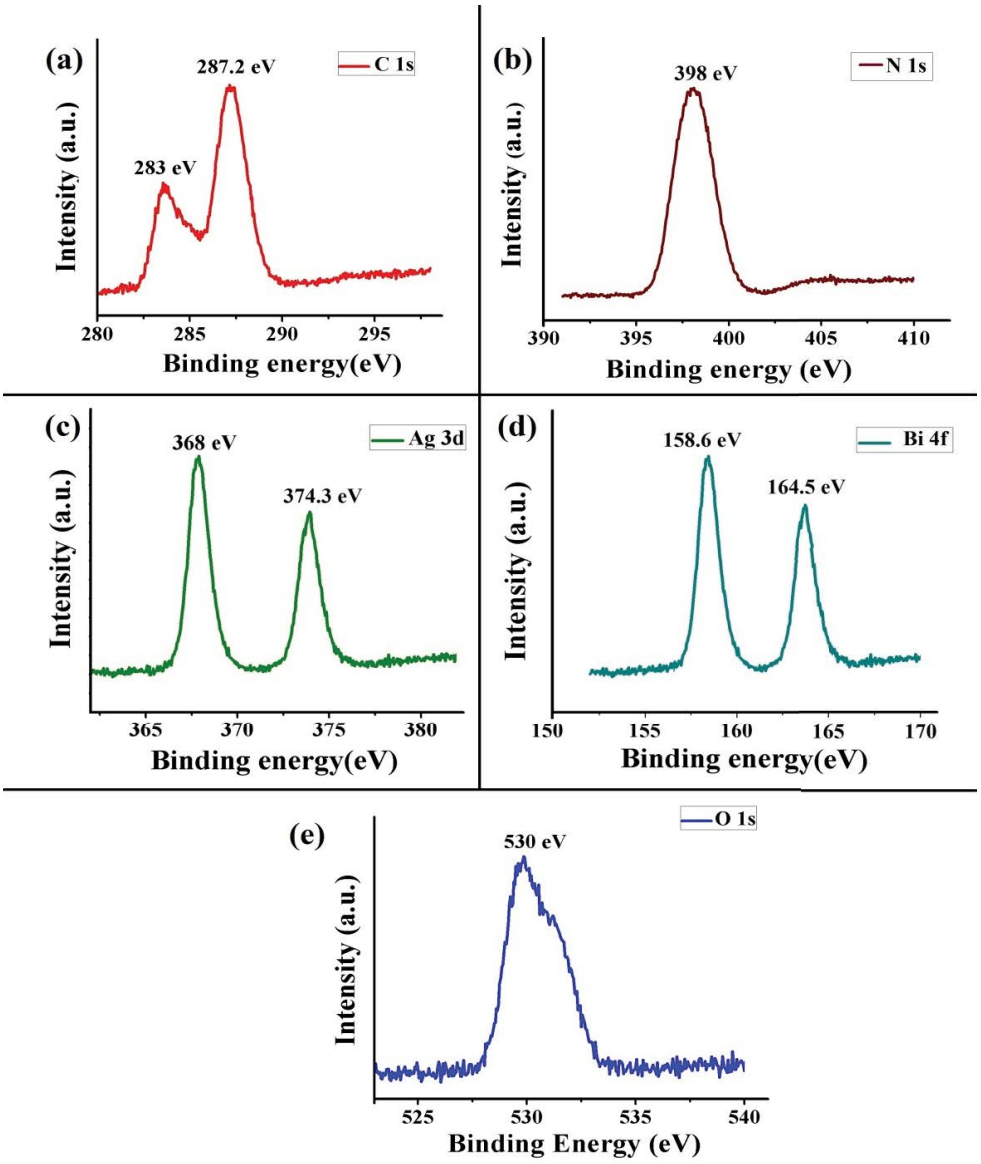

Fig. 5. XPS spectra showing presence of (a) C 1s, (b) N 1s, (c) Ag 3d, (d) Bi 4f, and (e) O1s elements of Ag-BO/GCN nanocomposite.

[47,48]. In Fig. 5e, peak for O 1s was observed at 530 eV due to lattice oxygen in Bi-O bonds [49].

Fig. 6a reveals optical properties of Ag-BO/GCN using UV–visible spectroscopy that exhibited significant absorption in visible light region. GCN and BO displayed strong absorption at approximately 459 and 442 nm, which were allocated to intrinsic band-gap absorption of GCN and BO (band gap of GCN is 2.7 eV and BO is 2.8 eV). In Ag-anchored BO, red shift was observed in absorption towards visible region compared with pure Bi_2O_3. The absorption bands were present in range of 500~700 nm in visible light region. The band gap energy of Ag-BO/GCN was estimated using Tauc's plots (Fig. 6b) having formula as follows [50,51]:

$$\alpha h\nu = A\left(h\nu - E_g\right)^{n/2} \quad (2)$$

where α indicates absorption coefficient near absorption edge, hν denotes photon energy, A is a constant, E_g signifies absorption band-gap energy and n designates different values on the basis of absorption process. Fig. 6b explores optical band gap by plotting straight curve between $(\alpha h\nu)^2$ vs. hν of nanocomposites. In this study, E_g was predicted by straight portion of $(\alpha h\nu)^2$ vs. hν, plotted to $\alpha = 0$,. The band gap of GCN, BO and Ag-BO/GCN was found to be 2.7, 2.8 and 2.3, respectively (Fig. 6b).

The PL spectra were used for the determination of charge trapping and photocatalytic efficiency in semiconductor. Fig. 6c illustrates PL spectrum of GCN, BO and Ag-BO, nanoparticles. The intensity of luminescence peak of Ag-anchored BO was weaker than bare BO and GCN, indicated in the figure. Semiconductor luminescence was mostly initiated by photogenerated electrons and holes recombination [51–54]. Thus, doping of Ag in BO successfully separated photogenerated electrons from holes on BO surface and subdued their recombination. Heterojunction of Ag-BO with GCN also enhanced separation of photogenerated charge carriers and thus improving activity of Ag-BO/GCN nanocomposites. pH_{zpc} of Ag-BO/GCN nanocomposite was calculated as 6.6 (Fig. 6d).

3.1. Photodegradation of imidacloprid (IMP) using Ag-BO/GCN photocatalyst

The photocatalytic ability of Ag-BO/GCN was examined for pesticide degradation under LED light irradiation. Fig. 7a depicts photodegradation and adsorptional removal of imidacloprid pesticide as a function of light irradiation time. In the absence of photocatalyst, photolysis had no effect on pesticide eradication. Under visible light, 93%, 71% and 65% IMP removal was observed for Ag-BO/GCN, Ag-BO and GCN, respectively. In the absence of light, 36%, 20% and 33% removal of IMP was recorded in 8 h. (Fig. 7b). The photocatalytic efficiency had followed the trend as: Ag-BO/GCN (light) > Ag-BO (light) ≈ GCN (light) > Ag-BO/GCN (dark) ≈ GCN (dark) > Ag-BO (dark). Ag-BO/GCN was the most effective photocatalyst for IMP degradation. Ag-BO/GCN and GCN had also substantial adsorption ability for IMP removal under dark. Ag-BO/GCN was the most competent photocatalyst and adsorbent for imidacloprid degradation.

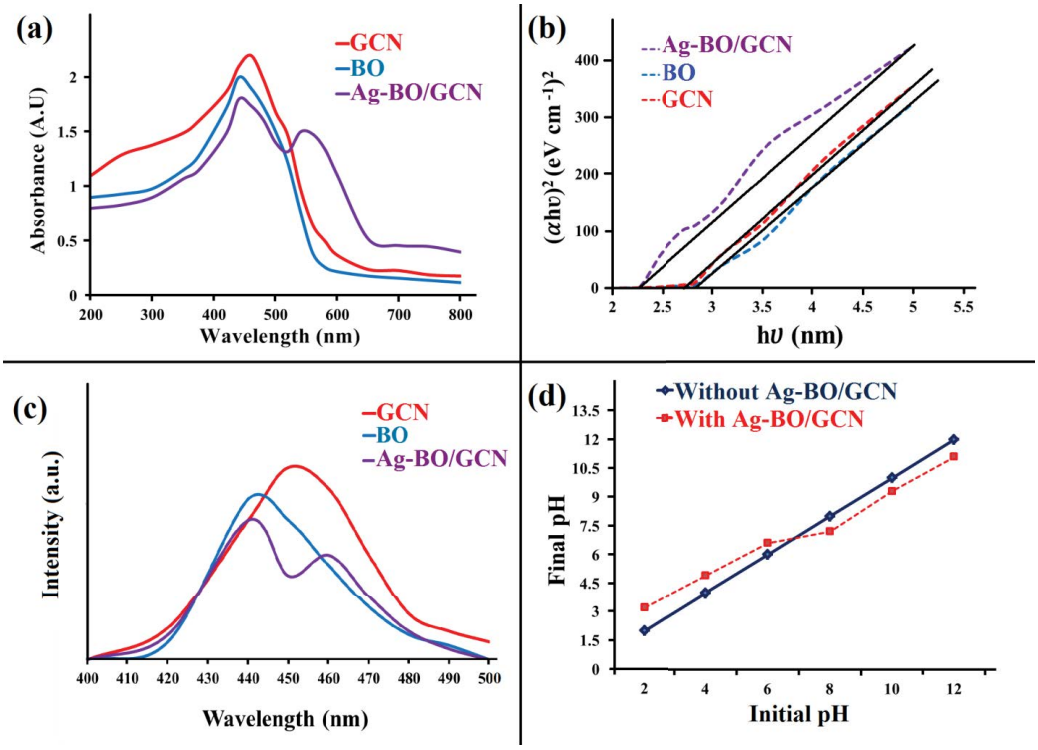

Fig. 6. UV–visible analysis (a), band gap calculations (b), photoluminiscenc of GCN, BO and Ag-BO/GCN (c) and pH_{zpc} with and without Ag-BO/GCN (d).

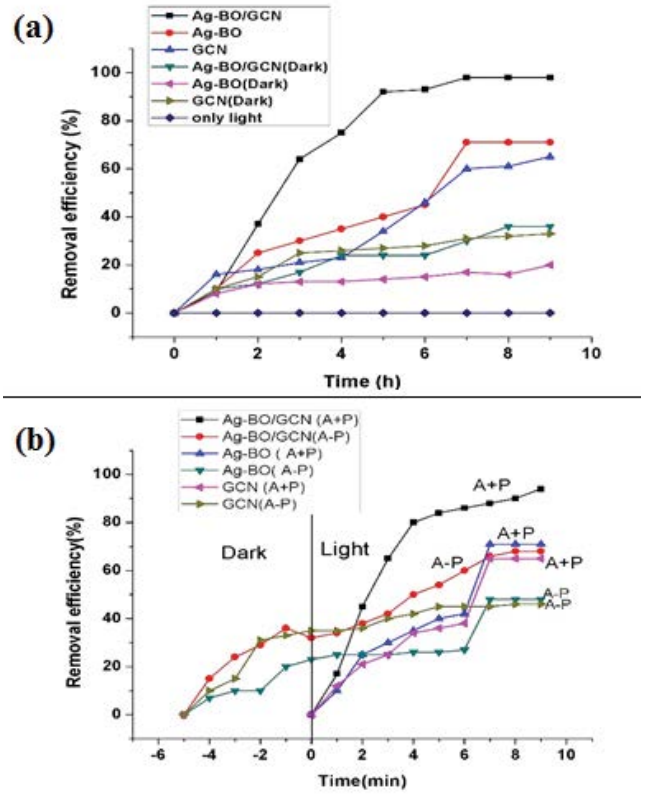

Fig. 7. Removal of IMP under different reaction conditions (a) and effect of adsorption on photocatalytic degradation of IMP (b). Reaction conditions: [IMP] = 1 × 10^{-4} mol dm^{-3}; [catalyst] = 50 mg/100 mL; initial reaction pH = 6.0; light intensity = 750 lx.

Moreover, IMP degradation was also subjected to instantaneous adsorption and photocatalysis (A + P) and adsorption followed by photocatalysis (A-P) to explore effect of adsorption on photodegradation using Ag-BO/GCN, Ag-BO and GCN photocatalyst as function of time in Fig. 7b. The first part of graph depicts IMP adsorption. During simultaneous adsorption and photocatalysis, 98%, 71% and 65% of IMP was photodegraded using Ag-BO/GCN, Ag-BO and GCN photocatalysts, respectively. While during A-P process, Ag-BO/GCN, Ag-BO and GCN had 68%, 48% and 46% removal efficiency for IMP degradation. During A + P, imidacloprid pesticide adsorbed onto photocatalyst surface was simultaneously oxidized by photocatalyst occurring in degradation process [55–59]. It caused enhancement in removal efficiency during A + P process, whereas, extreme adsorption of IMP during A-P process reduced irradiated light falling on photocatalyst surface causing a reduction in photoactive volume. The condensed photoactive dimensions instigated decease in photodegradation activity of photocatalysts. Furthermore, kinetics of IMP degradation was explored by given equation [60,61].

$$-\frac{dC}{dt} = kt \tag{3}$$

where C is IMP concentration at time t and k denotes rate constant value (Eq. (3)) can be written as:

$$-\ln\left(\frac{C}{C_0}\right) = kt \tag{4}$$

The graph was plotted between $-\ln(C/C_0)$ vs. time (t) for the determination of rate constants. The plots linearity confirmed pseudo-first order kinetics throughout the photodegradation path. Ag-BO/GCN/A + P, Ag-BO/A + P, GCN/A + P, Ag-BO/GCN/A-P, Ag-BO/A-P and GCN/A-P catalytic processes had rate constants of 0.090, 0.071, 0.062, 0.068, 0.47 and 0.049 min^{-1}, respectively. The obtained regression coefficient (R^2) values between 0.99 and 0.98 suggested pseudo-first order kinetics for degradation process (Table 1). The above investigation claims that Ag-BO/GCN/A + P catalytic system was most efficient for IMP degradation under visible light. Further studies were undertaken with Ag-BO/GCN/A + P.

3.2. Influence of initial IMP concentration, catalyst dose and pH on IMP degradation

The influence of catalyst loading on IMP degradation was explored by varying amount of photocatalyst during photocatalytic degradation (Table 2). The rate constant value increased from 0.091 to 0.17 min^{-1} with variation in photocatalyst dose from 10 to 70 mg/50 mL. The increment in rate constant was due to rise in number of active site that ultimately enhanced pollutant photodegradation process. However, further increase in Ag-BO/GCN loading resulted in decrease in IMP photodegradation. The reduction in photodegradation rate was due to decrease in photoactive volume owing to excess of catalyst present in reaction solution. The turbidity and agglomeration at the time of photocatalytic reaction reduced the photoactive volume. The basis of initial concentration of pollutant, number of collisions can be identified which is a rate determining factor and can be calculated from following equation:

$$r = kc \tag{5}$$

where r signifies reaction rate, k indicates reaction rate constant and c denotes pollutant concentration at time

Table 1
Value of rate constant for photodegradation of IMP under visible light

Photocatalytic process	Rate constant (k_1) min^{-1}	R^2	% Efficiency
Ag-BO/GCN/A + P	0.090	0.99	98
Ag-BO/A + P	0.071	0.96	71
GCN/A + P	0.062	0.95	65
Ag-BO/GCN/A-P	0.068	0.97	68
Ag-BO/A-P	0.047	0.96	46
GCN/A-P	0.049	0.98	48

Reaction conditions: [IMP] = 1 × 10^{-4} mol dm^{-3}; [catalyst] = 50 mg/100 mL; initial reaction pH = 6.0; time = 8 h and light intensity = 750 lx.

t. The initial concentration of imidacloprid was varied from 1.0 × 10^{-3} to 13.0 × 10^{-3} mol dm^{-3} (Table 2). The rise in rate constant was observed from 0.085 to 0.11 min^{-1} with increase in initial concentration of IMP from 1.0 × 10 to 7.0 × 10^{-4} mol dm^{-3}. The increase in rate constant was attributed to increase in number of effective collision [62]. Moreover, light scattering beyond optimal concentration resulted in decreased rate constant for IMP degradation [63].

Imidacloprid (IMP) is quite stable in water as well as in dark at 2.7, 5 and 8 pH and possesses no loss through chemical hydrolysis when kept for 10 h in solution. On increasing pH of solution from 2 to 13, rate constant for imidacloprid degradation decreased from 0.1 to 0.049 min. The change of pH also led to protonation and deprotonation. The zero point charge for Ag-BO/GCN was 6.90. The surface of photocatalyst was positively charged below pH < 6.90 and above pH_{zpc}, it was negatively charged. Because of the presence of electron-rich aromatic rings in imidacloprid molecule structure, it gets absorbed on the positively charged surface in acidic solutions. During experimental situations, imidacloprid photodegradation exhibited better efficiency in acidic solutions than alkaline solution.

3.3. Long-term mineralization and mechanistic view of IMP degradation

Imidacloprid pesticide was subjected to long-term mineralization using Ag-BO/GCN/A + P catalytic process. The mineralization extent was investigated by COD removal during degradation process (Fig. 8a). Ag-BO/GCN/A + P, Ag-BO/A + P and GCN/A + P catalytic processes displayed 96%, 65% and 50% COD elimination in 10 h (Fig. 8b) [64]. The mineralization of IMP was attended using Ag-BO/GCN/A + P catalytic system. Usually, hydroxyl radicals (•OH), holes (h^+_{VB}), superoxide radicals ($•O_2^-$), electrons (e_{CB}^-) are the main reactive species for photocatalytic degradation processes. In the present work, ammonium oxalate (AO) as hole scavengers [65–67], isopropanol (IPA) as hydroxyl free radical (•OH) scavengers [68,69] and benzoquinone (BQ) as superoxide radical ($•O_2^-$) were used to find reactive species during oxidation process [70] (Fig. 8c). The removal efficiency was reduced to 10% and 13% from 70% on addition of IPA and BZQ, respectively. The scavenging results confirmed •OH and $•O_2^-$ radicals as main oxidants for IMP degradation.

GCN has more negative potential (E_0 = –1.12 eV) as compared with $O_2/•O_2^-$ potential (E_0 (O_2/ $•O_2^-$) which is equal to −0.33 eV/NHE. However, photogenerated holes in GCN (h^+)

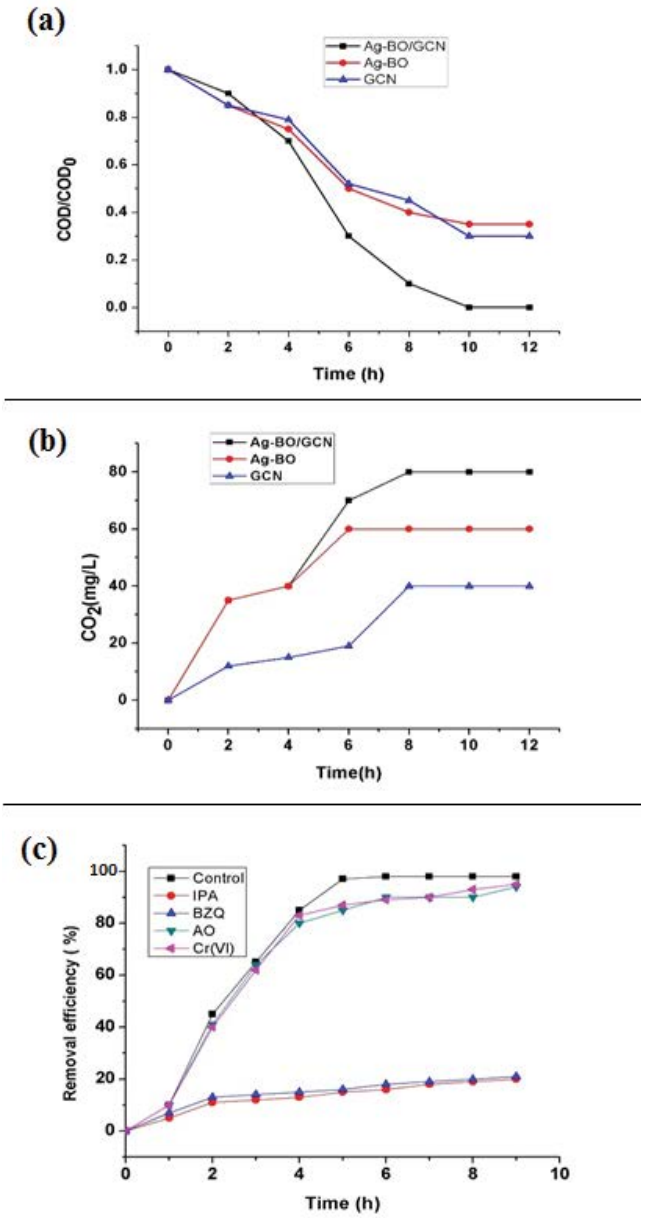

Fig. 8. COD removal during degradation process (a–b) and effect of scavengers on photocatalytic degradation of IMP (c).

Table 2
Effect of reaction parameters on IMP degradation

Catalyst loading	Catalyst loading (mg/50 mL)	10.0	30.0	50.0	70.0	90.0	110.0	130.0
	k_1 (min^{-1})	0.091	0.096	0.1	0.17	0.093	0.090	0.081
Initial IMP	Concentration (10^{-4} mol dm^{-3})	1.0	3.0	5.0	7.0	9.0	11.0	13.0
concentration	k_1 (min^{-1})	0.085	0.088	0.091	0.11	0.094	0.087	0.084
pH	pH	2.0	4.0	6.0	7.0	8.0	10.0	12.0
	k_1 (min^{-1})	0.12	0.1	0.091	0.074	0.069	0.055	0.049

Reaction parameters: [IMP] = 1 × 10^{-4} mol dm^{-3}; [catalyst] = 50 mg/100 mL; initial reaction pH = 6.0; time = 10 h and solar light intensity = 750 lx.

did not produce hydroxyl radicals due to lower VB potential (E_0 = –1.12 eV) than (E_0 (•OH, H^+/H_2O) = 2.72 eV/NHE). Ag-BO/GCN heterojunction leads to reduction in electron–hole pair recombination due to Ag(0) that stores and transfers electron between GCN and BO photocatalyst. Upon heterojunction formation with BO, photogenerated electrons from the conduction band of BO were shifted to the VB of GCN through Ag(0) mediated Z scheme transfer. At the same time, remaining holes in the VB of BO reacted with H_2O to produce •OH radicals because E_{VB} of BO (3.13 eV νs NHE) was more positive than •OH/H_2O (+1.99 eV). While photogenerated electrons in CB of GCN reacted with molecular oxygen to produce superoxide radicals ($•O_2^-$). The superoxide radicals combined with H^+ ions to produce •OH radicals. Under visible light exposure, e^- present in CB of GCN with sufficient reduction potential produce $•O_2^-$ radicals via reacting with O_2 which in turn either directly react with imidacloprid or produce •OH radicals by reacting with H^+ ion in further reaction. On the other hand, the spatially separated h^+ (VB) in BO possess optimal potential to generate •OH radicals by reacting with H_2O. Thereby, formation of Z-scheme heterojunction mediated by Ag leads to the space separation of photocarriers with apt redox potential to facilitate the photoinduced surface reactions. Thus, superoxide radicals $•O_2^-$ and •OH reacted with IMP to produce degraded products (Fig. 9).

3.4. Recyclability of Ag-BO/GCN

Recyclability and stability of nanocomposite play a significant role in actual time application of photocatalyst. The recycle efficacy of Ag-BO/GCN nanocomposite was explored for 10 consecutive catalytic cycles (Fig. 10a). Efficiency of Ag-BO/GCN nanocomposite was deflated to 88% from 98% for imidacloprid pesticide degradation. Although no major changes in morphology were seen in SEM, EDX of Ag-BO/GCN nanocomposite (Figs. 10b–d). Thus, the obtained results undoubtedly displayed implausible stability of Ag-BO/GCN nanocomposites completed with 10 consecutive cycles for the eradication of imidacloprid pesticide.

4. Conclusion

Ag-BO/GCN nanocomposites with enhanced photocatalytic activity were synthesized via thermal polycondensation method and one-step hydrothermal method as well as used for pollutant eradication from wastewater. FESEM and HRTEM analysis clearly indicated the formation of heterojunction of g-C_3N_4 with Ag-anchored BO. The XPS, XRD and FTIR analysis depicted successful formation of Ag-BO/GCN nanocomposites. The optical band gap of g-C_3N_4 and

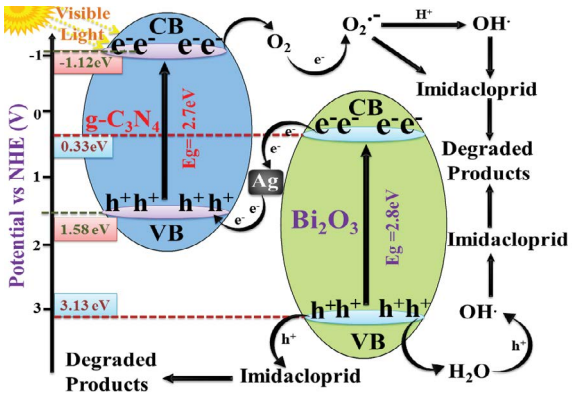

Fig. 9. Mechanistic view of IMP degradation using Ag-BO/GCN photocatalyst.

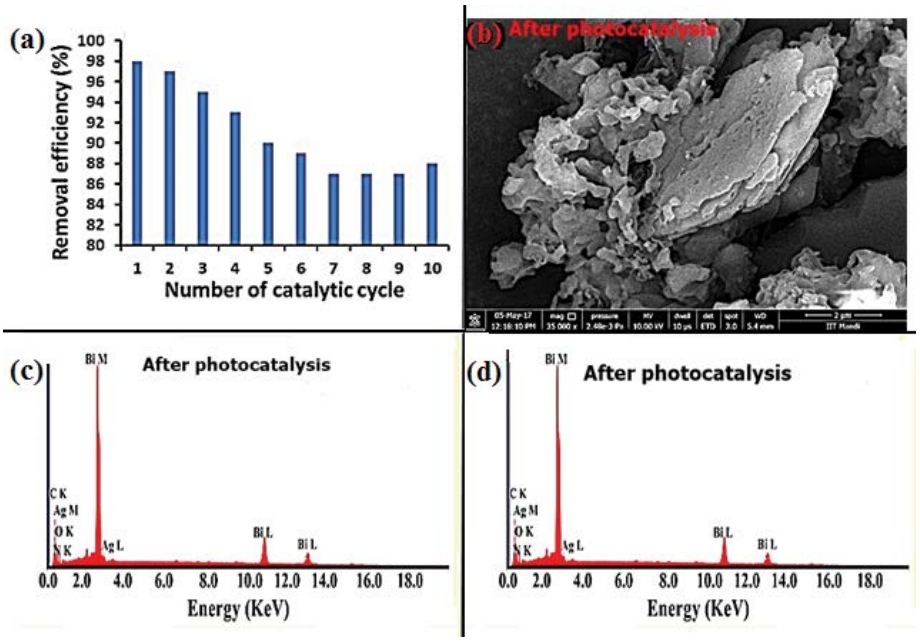

Fig. 10. Recycle efficiency of Ag-BO/GCN photocatalyst (a), SEM image and EDX analysis after photocatalytic process (b–d). [IMP] = 1 × 10^{-4} mol dm^{-3}; [catalyst] = 50 mg/100 mL; initial reaction pH = 6.0; reaction time = 10 h; light intensity = 750 lx.

Ag-anchored BO was found to be 2.3 eV. The heterojunction formation of g-C_3N_4 with Ag-anchored BO involved the effective separation of photogenerated electron–hole pairs and more absorption of visible light irradiation. IMP degradation followed pseudo-first order kinetics. Ag-BO/GCN exhibited substantial photocatalytic activity for 10 catalytic cycles. IMP was completely mineralized in 10 h under visible light. Hydroxyl radicals (•OH) and holes (h^+_{VB}) were two main reactants involved in m oxidative degradation of IMP. No major loss in photocatalytic activity was found after 10 catalytic cycles. The prepared photocatalysts showed significant recyclability for 10 catalytic cycles.

References

[1] Q. Zheng, D.P. Durkin, J.E. Elenewski, Y. Sun, N.A. Banek, L. Hua, H. Chen, M.J. Wagner, W. Zhang, D. Shuai, Visible-light-responsive graphitic carbon nitride: rational design and photocatalytic applications for water treatment, Environ. Sci. Technol., 50 (2016) 12938–12948.

[2] P. Singh, B. Priya, P. Shandilya, P. Raizada, N. Singh, B. Pare, S.B. Jonnalagadda. Photocatalytic mineralization of antibiotics using 60% WO_3/BiOCl stacked to graphene sand composite and chitosan, Arab. J. Chem., (2016), (In Press), https://doi.org/10.1016/j.arabjc.2016.08.005.

[3] A. Fujishima, K. Honda, Electrochemical photolysis of water at a semiconductor electrode, Nature, 238 (1972) 37.

[4] H. Cao, Y. Zhu, X. Tan, H. Kang, X. Yang, C. Li, Fabrication of TiO_2/CdS composite fiber via an electrospinning method, New J. Chem., 34 (2010) 1116–1119.

[5] S.C. Yan, S.B. Lv, Z.S. Li, Z.G. Zou, Organic–inorganic composite photocatalyst of g-C_3N_4 and TaON with improved visible light photocatalytic activities, Dalton Trans., 39 (2010) 1488–1491.

[6] V. Hasija, P. Raizada, A. Sudhaik, K. Sharma, A. Kumar, P. Singh, S.B. Jonnalagadda, V.K. Thakur, Recent advances in noble metal free doped graphitic carbon nitride based nanohybrids for photocatalysis of organic contaminants in water: a review, Appl. Mater. Today, 15 (2019) 494–524.

[7] A. Habibi-Yangjeh, M. Mousavi, Deposition of $CuWO_4$ nanoparticles over g-C_3N_4/Fe_3O_4 nanocomposite: novel magnetic photocatalysts with drastically enhanced performance under visible-light, Adv. Powder Technol., 29 (2018) 1379–1392.

[8] S. Sharma, V. Dutta, P. Singh, P. Raizada, A. Rahmani-Sani, A. Hosseini-Bandegharaei, V. Kumar Thakur, Carbon quantum dot supported semiconductor photocatalysts for efficient degradation of organic pollutants in water: a review, J. Clean. Prod., 228 (2019) 755–769.

[9] P. Shandilya, D. Mittal, M. Soni, P. Raizada, A. Hosseini-Bandegharaei, A.K. Saini, P. Singh, Fabrication of fluorine doped graphene and $SmVO_4$ based dispersed and adsorptive photocatalyst for abatement of phenolic compounds from water and bacterial disinfection, J. Clean. Prod., 203 (2018) 386–399.

[10] W.T. Dong, C.S. Zhu, Optical properties of surface-modified BO nanoparticles, J. Phys. Chem. Solids, 64 (2003) 265–271.

[11] B. Priya, P. Raizada, N. Singh, P. Thakur, P. Singh, Adsorptional photocatalytic mineralization of oxytetracycline and ampicillin antibiotics using BO/BiOCl supported on graphene sand composite and chitosan, J. Colloid Interface Sci., 479 (2016) 271–283.

[12] P. Raizada, A. Sudhaik, P. Singh, P. Shandilya, V.K. Gupta, A.H. Bandegharaei, S. Agrawal, Ag_3PO_4 modified phosphorus and sulphur co-doped graphitic carbon nitride as a direct Z-scheme photocatalyst for 2, 4-dimethyl phenol degradation, J. Photochem. Photobiol. A: Chem., 374 (2019) 22–35.

[13] R. Chen, Z.R. Shen, H. Wang, H.J. Zhou, Y.P. Liu, D.T. Ding, T.H. Chen, Fabrication of mesh-like bismuth oxide single crystalline nanoflakes and their visible light photocatalytic activity, J. Alloys Comp., 9 (2011) 2588–2596.

[14] S. Iyyapushpam, S.T. Nishanthi, D.P. Padiyan, Photocatalytic degradation of methyl orange using α-BO prepared without surfactant, J. Alloys Comp., 563 (2013) 104–107.

[15] K. Sharma, V. Dutta, S. Sharma, P. Raizada, A. Hosseini-Bandegharaei, P. Thakur, P. Singh, Recent advances in enhanced photocatalytic activity of bismuth oxyhalides for efficient photocatalysis of organic pollutants in water: a review, J. Ind. Eng. Chem., 78 (2019) 1–20.

[16] M.L. Guan, D.K. Ma, S.W. Hu, Y.J. Chen, S.M. Huang, From hollow olive-shaped $BiVO_4$ to n-p Core-Shell $BiVO_4$@ BO microspheres: controlled synthesis and enhanced visible-light-responsive photocatalytic properties, Inorg. Chem., 50 (2010) 800–805.

[17] J. Zhu, S. Wang, J. Wang, D. Zhang, H. Li, Highly active and durable BO/TiO_2 visible photocatalyst in flower-like spheres with surface-enriched BO quantum dots, Appl. Catal., B, 102 (2011) 120–125.

[18] A. Sudhaik, P. Raizada, P. Shandilya, D.Y. Jeong, J.H. Lim, P. Singh, Review on fabrication of graphitic carbon nitride based efficient nanocomposites for photodegradation of aqueous phase organic pollutants, J. Ind. Eng. Chem., 67 (2018) 28–51.

[19] X. Wang, K. Maeda, A. Thomas, K. Takanabe, G. Xin, J.M. Carlsson, K. Domen, M. Antonietti, A metal-free polymeric photocatalyst for hydrogen production from water under visible light, Nat. Mater., 8 (2009) 76–80.

[20] S. Asadzadeh-Khaneghah, A. Habibi-Yangjeh, D. Seifzadeh, Graphitic carbon nitride nanosheets coupled with carbon dots and BiOI nanoparticles: boosting visible-light-driven photocatalytic activity, J. Taiwan Inst. Chem. Eng., 87 (2018) 98–111.

[21] S. Asadzadeh-Khaneghah, A. Habibi-Yangjeh, M. Abedi, Decoration of carbon dots and AgCl over g-C_3N_4 nanosheets: novel photocatalysts with substantially improved activity under visible light, Sep. Purif. Technol., 199 (2018) 64–77.

[22] Y. Zhou, L. Zhang, J. Liu, X. Fan, B. Wang, M. Wang, W. Ran, J. Wang, M. Li, J. Shi, Brand new P-doped g-C_3N_4: enhanced photocatalytic activity for H_2 evolution and Rhodamine B degradation under visible light, J. Mater. Chem. A, 3 (2015) 3862–3867.

[23] S. Asadzadeh-Khaneghah, A. Habibi-Yangjeh, K. Nakata, Decoration of carbon dots over hydrogen peroxide treated graphitic carbon nitride: exceptional photocatalytic performance in removal of different contaminants under visible light, J. Photochem. Photobiol. A: Chem., 374 (2019) 161–172.

[24] P. Raizada, A. Sudhaik, P. Singh, P. Shandilya, A.K. Saini, V.K. Gupta, J.H. Lim, H. Jung, A.H. Bandegharaei, Fabrication of Ag_3VO_4 decorated phosphorus and sulphur co-doped graphitic carbon nitride as a high-dispersed photocatalyst for phenol mineralization and *E. coli* disinfection, Sep. Purif. Technol., 212 (2019) 887–900.

[25] P. Shandilya, D. Mittal, A. Sudhaik, M. Soni, P. Raizada, A.K. Saini, P. Singh, $GdVO_4$ modified fluorine doped graphene nanosheets as dispersed photocatalyst for mitigation of phenolic compounds in aqueous environment and bacterial disinfection, Sep. Purif. Technol,. 210 (2019) 804–816.

[26] B. Pare, P. Singh, S.B. Jonnalagadda, Degradation and mineralization of victoria blue B dye in a slurry photoreactor using advanced oxidation process, J. Sci. Ind. Res., 68 (2009) 724–729.

[27] B. Pare, P. Singh, S.B. Jonnalagadda, Visible light induced heterogeneous advanced oxidation process to degrade pararosanilin dye in aqueous suspension of ZnO, Ind. J. Chem. Sect. A, 47 (2008) 830–835.

[28] P. Raizada, A. Sudhaik, P. Singh, A. Hosseini-Bandegharaei, P. Thakur, Converting type II AgBr/VO into ternary Z scheme photocatalyst via coupling with phosphorus doped g-C_3N_4 for enhanced photocatalytic activity, Sep. Purif. Technol., 227 (2019) 115692.

[29] C. Wang, C. Shao, Y. Liu, L. Zhang, Photocatalytic properties BiOCl and BO nanofibers prepared by electrospinning, Scripta Mater., 59 (2008) 332–335.

[30] Y. Li, S. Wu, L. Huang, H. Xu, R. Zhang, M. Qu, Q. Gao, H. Li, GCN modified BO composites with enhanced visible-light photocatalytic activity, J. Phys. Chem. Solid, 76 (2015) 112–119.

[31] Y. Zhang, J. Lu, M.R. Hoffmann, Q. Wang, Y. Conga, Q. Wang, H. Jin, Synthesis of GCN/BO/TiO_2 composite nanotubes:

Enhanced activity under visible light irradiation and improved photoelectrochemical activity, RSC Adv., 5 (2015) 48983–48991.
[32] L. Huang, H. Xu, Y. Li, H. Li, X. Cheng, J. Xia, Y. Xu, G. Cai, Visible-light-induced WO_3/GCN composites with enhanced photocatalytic activity, Dalton Trans., 42 (2013) 8606–8616.
[33] T. Tyborski, C. Merschjann, S. Orthmann, F. Yang, M.C. Lux-Steiner, T. Schedel-Niedrig, Tunable optical transition in polymeric carbon nitrides synthesized via bulk thermal condensation, J. Phys.: Condens. Matter, 24 (2012) 162201.
[34] J. Zhang, Y. Li, P. Zhu, D. Huang, S. Wu, Q. Cui, G. Zou, Graphitic carbon nitride materials synthesized via reactive pyrolysis routes and their properties, Diam. Relat. Mater., 20 (2011) 385–388.
[35] A.F. Gualtieri, S. Immovilli, M. Prudenziati, Powder X-ray diffraction data for the new polymorphic compound ω-BO, Powder Diffr., 12 (1997) 90–92.
[36] O. Pawar, N. Deshpande, S. Dagade, S. Waghmode, P.N. Joshi, Green synthesis of silver nanoparticles from purple acid phosphatase apoenzyme isolated from a new source, *Limonia acidissima*, J. Exp. Nanosci., 11 (2015) 28–37.
[37] H. Katsumata, Y. Tachi, T. Suzuki, S. Kaeco, Z-scheme photocatalytic hydrogen production over WO_3/g-C_3N_4 composite photocatalysts, RSC Adv., 4 (2014) 21405–21409.
[38] S. Kumar, T. Surendar, B. Kumar, A. Baruah, V. Shanker, Synthesis of magnetically separable and recyclable g-C_3N_4/Fe_3O_4 hybrid nanocomposites with enhanced photocatalytic performance under visible-light irradiation, J. Phys. Chem. C, 117 (2013) 26135–26143.
[39] Q. Zhuang, L. Sun, Y. Ni, One-step synthesis of graphitic carbon nitride nanosheets with the help of melamine and its application for fluorescence detection of mercuric ions, Talanta, 164 (2017) 458–462.
[40] R. Irmawati, M.N.N. Nasriah, Y.H. Taufig-Yap, S.B.A. Hamid, Characterization of bismuth oxide catalysts prepared from bismuth trinitrate pentahydrate: influence of bismuth concentration, Catal. Today, 93–95 (2004) 701–709.
[41] V. Fruth, M. Popa, D. Berger, C.M. Ionica, M. Jitianu, Phases investigation in the antimony doped BO system, J. Eur. Ceram. Soc., 24 (2004) 1295–1299.
[42] S.R.G. Carrazan, C. Martin, V. Rives, R. Vidal, An FT-IR spectroscopy study of the adsorption and oxidation of propene on multiphase Bi, Mo and Co catalysts, Spectrochim. Acta Part A, 52 (1996) 1107–1118.
[43] M. Faisal, S.B. Khan, M.M. Rahman, A. Jamal, M.M. Abdullah, Fabrication of ZnO nanoparticles based sensitive methanol sensor and efficient photocatalyst, Appl. Surf. Sci., 258 (2012) 7515–7522.
[44] S.B. Khan, M. Faisal, M.M. Rahman, A. Jamal, Low-temperature growth of ZnO nanoparticles: photocatalyst and acetone sensor, Talanta, 85 (2011) 943–949.
[45] P. Niu, G. Liu, H.M. Cheng, Nitrogen vacancy-promoted photocatalytic activity of graphitic carbon nitride, J. Phys. Chem. C, 116 (2012) 11013–11018.
[46] S. Ma, S. Zhan, Y. Jia, Q. Shi, Q. Zhou, Enhanced disinfection application of Ag-modified g-C_3N_4 composite under visible light, Appl. Catal., B, 186 (2016) 77–87.
[47] W.J. Shan, Y. Hu, Z.G. Bai, M.M. Zheng, C.H. Wei, In situ preparation of g-C_3N_4/ bismuth-based oxide nanocomposites with enhanced photocatalytic activity, Appl. Catal., B, 188 (2016) 1–12.
[48] M. Sun, Y. Wang, Y. Shao, Y.H. He, Q. Zheng, H.K. Liang, T. Yan, B. Du, Fabrication of a novel Z-scheme g-C_3N_4/Bi_4O_7 heterojunction photocatalyst with enhanced visible light-driven activity toward organic pollutants, J. Colloid Interface Sci., 501 (2017) 123–132.
[49] H. Zou, M.X. Song, F.C. Yi, L. Bian, P. Liu, S. Zhang, Simulated-sunlight-activated photocatalysis of Methyl Orange using carbon and lanthanum co-doped BO-TiO_2 composite, J. Alloy. Compd., 680 (2016) 54–59.
[50] S. Gautam, P. Shandilya, B. Priya, V.P. Singh, P. Raizada, R. Rai, M.A. Valente, P. Singh, Superparamagnetic $MnFe_2O_4$ dispersed over graphitic carbon sand composite and bentonite as magnetically recoverable photocatalyst for antibiotic mineralization, Sep. Purif. Technol., 172 (2017) 498–511.
[51] P. Shandilya, D. Mittal, M. Soni, P. Raizada, J.H. Lim, D.Y. Jeong, R.P. Dewedi, A.K. Saini, P. Singh, Islanding of $EuVO_4$ on high-dispersed fluorine doped few layered graphene sheets for efficient photocatalytic mineralization of phenolic compounds and bacterial disinfection, J. Taiwan Inst. Chem. Eng., 93 (2018) 528–542.
[52] P. Raizada, J. Kumari, P. Shandilya, R. Dhiman, V.P. Singh, P. Singh, Magnetically retrievable Bi_2WO_6/Fe_3O_4 immobilized on graphene sand composite for investigation of photocatalytic mineralization of oxytetracycline and ampicillin, Process Saf. Environ. Prot., 106 (2017) 104–116.
[53] A. Sudhaik, P. Raizada, P. Shandilya, P. Singh, Magnetically recoverable graphitic carbon nitride and $NiFe_2O_4$ based magnetic photocatalyst for degradation of oxytetracycline antibiotic in simulated wastewater under solar light, J. Environ. Chem. Eng., 6 (2018) 3874–3883.
[54] P. Raizada, B. Priya, P. Thakur, P. Singh, Solar light induced photodegradation of oxytetracycline using Zr doped TiO_2/CaO based nanocomposite, Indian J. Chem., 55 (2016) 803–809.
[55] S. Ahmed, M.G. Rasul, R. Brown, M.A. Hashib, Influence of parameters on the heterogeneous photocatalytic degradation of pesticides and phenolic contaminants in wastewater: a short review, J. Environ. Manage., 92 (2011) 311–330.
[56] W. Bahnemann, M. Muneer, M.M. Haque, Titanium dioxide-mediated photocatalysed degradation of few selected organic pollutants in aqueous suspensions, Catal. Today, 124 (2007) 133–148.
[57] J.M. Herrmann, Heterogeneous photocatalysis: fundamentals and applications to the removal of various types of aqueous pollutants, Catal. Today, 53 (1999) 115–129.
[58] N. Daneshvar, S. Aber, A. Khani, A.R. Khataee, Study of imidacloprid removal from aqueous solution by adsorption onto granular activated carbon using an on–line spectrophotometric analysis system, J. Hazard. Mater., 144 (2007) 47–51.
[59] P. Singh, Sonu, P. Raizada, A. Sudhaik, P. Shandilya, P. Thakur, S. Agarwal, V.K. Gupta, Enhanced photocatalytic activity and stability of AgBr/BiOBr/graphene heterojunction for phenol degradation under visible light, J. Saudi Chem. Soc., 23 (2018) 586–599.
[60] P. Raizada, P. Singh, A. Kumar, G. Sharma, B. Pare, S.B. Jonnalagadda, P. Thakur, Solar photocatalytic activity of nano-ZnO supported on activated carbon or brick grain particles: role of adsorption in dye degradation, Appl. Catal., A, 486 (2014) 159–169.
[61] B. Priya, P. Shandilya, P. Raizada, P. Thakur, N. Singh, P. Singh, Photocatalytic mineralization and degradation kinetics of ampicillin and oxytetracycline antibiotics using graphene sand composite and chitosan supported BiOCl, J. Mol. Catal. A, 423 (2016) 400–413.
[62] P. Raizada, A. Sudhaik, P. Singh, P. Shandilya, P. Thakur, H. Jung, Visible light assisted photodegradation of 2, 4-dinitrophenol using Ag_2CO_3 loaded phosphorus and sulphur co-doped graphitic carbon nitride nanosheets in simulated wastewater, Arab. J. Chem., (2018), (In Press), https://doi.org/10.1016/j.arabjc.2018.10.004.
[63] B. Pare, S.B. Jonnalagadda, H. Tomar, P. Singh, V.W. Bhagwat, ZnO assisted photocatalytic degradation of acridine orange in aqueous solution using visible irradiation, Desalination, 232 (2008) 80–90.
[64] T. Ding, D. Jacobs, B. Lavine, Liquid chromatography-mass spectrometry identification of imidacloprid photolysis products, Microchem. J., 99 (2011) 535–541.
[65] M. Turabik, N. Oturan, B. Gözmen, M.A. Oturan, Efficient removal of insecticide "imidacloprid" from water by electrochemical advanced oxidation processes, Environ. Sci. Pollut. Res., 21 (2014) 8387–8397.
[66] S.F. Chen, Y.F. Hu, S.G. Meng, X.L. Fu, Study on the separation mechanisms of photogenerated electrons and holes for composite photocatalysts g-C_3N_4-WO_3, Appl. Catal., B, 150–151 (2014) 564–573.
[67] H.X. Zhao, H.T. Yu, X. Quan, S. Chen, Y.B. Zhang, H.M. Zhao, H. Wang, Fabrication of atomic single layer graphitic-C_3N_4

and its high performance of photocatalytic disinfection under visible light irradiation, Appl. Catal., B, 152–153 (2014) 46–50.
[68] S.C. Yan, Z.S. Li, Z.G. Zou, Photodegradation of Rhodamine B and methyl orange over boron-doped g-C_3N_4 under visible light irradiation, Langmuir, 26 (2010) 3894–3901.
[69] H. Lee, W.Y. Choi, Photocatalytic oxidation of arsenite in TiO_2 suspension: kinetics and mechanisms, Environ. Sci. Technol., 36 (2002) 3872–3878.
[70] W.J. Li, D.Z. Li, Y.M. Lin, P.X. Wang, W. Chen, X.Z. Fu, Y. Shao, Evidence for the active species involved in the photodegradation process of methyl orange on TiO_2, J. Phys. Chem. C, 116 (2012) 3552–3560.

Supplementary information:

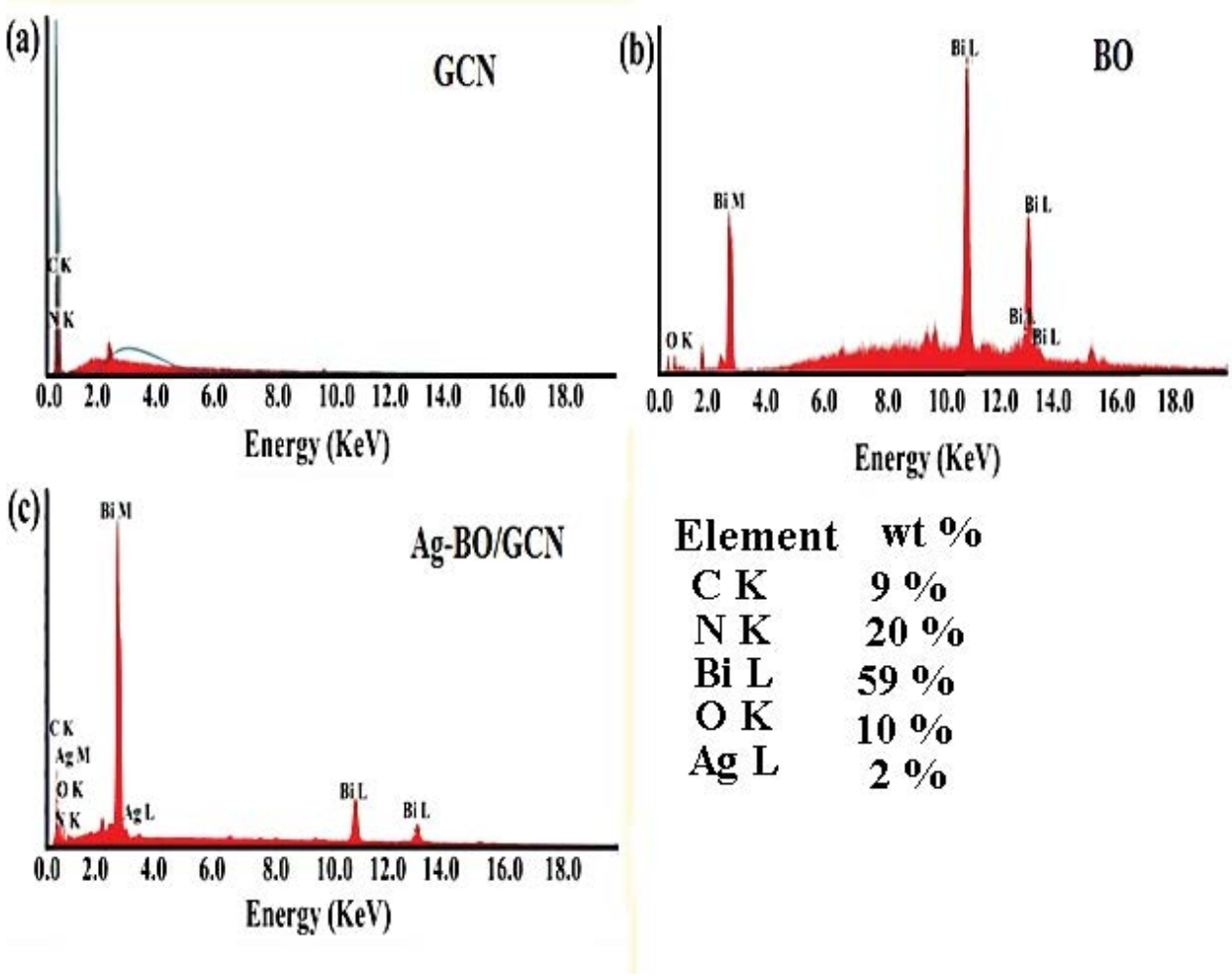

Fig. S1. EDX spectra of GCN BO and Ag-BO/GCN.